International Journal of Nanomedicine

Dovepress
open access to scientific and medical research

Open Access Full Text Article

ORIGINAL RESEARCH

Antiviral potential of green synthesized silver nanoparticles of *Lampranthus coccineus* and *Malephora lutea*

This article was published in the following Dove Press journal:
International Journal of Nanomedicine

Eman G Haggag[1]
Ali M Elshamy[2]
Mohamed A Rabeh[2,3]
Nagwan M Gabr[1]
Mohamed Salem[4]
Khayrya A Youssif[3]
Ahmed Samir[4]
Abdullatif Bin Muhsinah[5]
Abdulrhman Alsayari[5]
Usama Ramadan Abdelmohsen[6]

[1]Department of Pharmacognosy, Faculty of Pharmacy, Helwan University, Cairo 11795, Egypt; [2]Department of Pharmacognosy, Faculty of Pharmacy, Cairo University, Cairo 11562, Egypt; [3]Department of Pharmacognosy, Faculty of Pharmacy, Modern University for Technology and Information, Cairo, Egypt; [4]Department of Pharmaceutical Chemistry, October University for Modern Sciences and Arts (Msa), Cairo, Egypt; [5]Department of Pharmacognosy, College of Pharmacy, King Khalid University, Abha 61441, Saudi Arabia; [6]Department of Pharmacognosy, Faculty of Pharmacy, Minia University, Minia, Egypt

Correspondence: Mohamed A Rabeh
Department of Pharmacognosy, Faculty of Pharmacy, Cairo University, Cairo 11562, Egypt
Email mohamedabdelatty68@yahoo.com

Usama Ramadan Abdelmohsen
Department of Pharmacognosy, Faculty of Pharmacy, Minia University, Minia 61519, Egypt
Email Usama.ramadan@mu.edu.eg

Background: Viral and microbial infections constitute one of the most important life-threatening problems. The emergence of new viral and bacterial infectious diseases increases the demand for new therapeutic drugs.

Purpose: The objective of this study was to use the aqueous and hexane extracts of *Lampranthus coccineus* and *Malephora lutea* F. Aizoaceae for the synthesis of silver nanoparticles, and to investigate its possible antiviral activity. In addition to the investigation of the phytochemical composition of the crude methanolic extracts of the two plants through UPLC-MS metabolomic profiling, and it was followed by molecular docking in order to explore the chemical compounds that might contribute to the antiviral potential.

Methods: The formation of SNPs was further confirmed using a transmission electron microscope (TEM), UV-Visible spectroscopy and Fourier transform infrared spectroscopy. The antiviral activity of the synthesized nanoparticles was evaluated using MTT assay against HSV-1, HAV-10 virus and Coxsackie B4 virus. Metabolomics profiling was performed using UPLC-MS and molecular docking was performed via Autodock4 and visualization was done using the Discovery studio.

Results: The early signs of SNPs synthesis were detected by a color change from yellow to reddish brown color. The TEM analysis of SNPs showed spherical nanoparticles with mean size ranges between 10.12 nm to 27.89 nm, and 8.91 nm 14.48 nm for *Lampranthus coccineus* and *Malephora lutea* aqueous and hexane extracts respectively. The UV-Visible spectrophotometric analysis showed an absorption peak at λmax of 417 nm.The green synthesized SNPs of *L. coccineus* and *M. lutea* showed remarkable antiviral activity against HSV-1, HAV-10, and CoxB4 virus. Metabolomics profiling of the methanolic extract of *L. coccineus* and *M. lutea* resulted in identifying 12 compounds. The docking study predicted the patterns of interactions between the compounds of *L. coccineus* and *M. lutea* with herpes simplex thymidine kinase, hepatitis A 3c proteinase, and Coxsackievirus B4 3c protease, which was similar to those of the co-crystal inhibitors and this can provide a supposed explanation for the antiviral activity of the aqueous and nano extracts of *L. coccineus* and *M. lutea*.

Conclusion: These results highlight that SNPs of *L. coccineus* and *M. lutea* could have antiviral activity against HSV-1, HAV-10, and CoxB4 virus.

Keywords: silver nanoparticles, antiviral, metabolomics profiling, *Lampranthus coccineus*, *Malephora lutea*

Introduction

Nanotechnology was developed for more than two decades, and this unique technology attracted the interest of scientists around the world.[1] Nanoparticles are defined as particles with dimensions <100 nm and have attracted much attention

due to their unique properties. Their physical (eg, plasmonic resonance, fluorescent enhancement) and chemical (eg, catalytic activity enhancement) properties derived from the high quantity of surface atoms and the high area/volume relation, as their diameter decreases, their surface area increases dramatically and as a consequence there is an increase over the original properties of their bulk materials.[2] Silver nanoparticles (SNPs) are one of the most successful symbols of noble nanoparticles that are being applied in many areas of life including food packaging, water filter, cosmetics, and therapeutic applications, eg, bio-labeling, bio-sensing, tumor imaging, and drug delivery.[3–6] SNPs have not only revealed unique properties of metallic nanoparticles but also had high antimicrobial activity, so they have been paid special attention of scientists and technologists for the development of different products against infectious pathogens.[7–9] Many research articles have demonstrated that SNPs are an effective biocidal agent against a wide range of Gram-negative and Gram-positive bacteria, even multidrug-resistant bacteria and fungal pathogens.[7–12] Shanmuganathan et al[13] proved the antimicrobial efficacies of the unconjugated SNPs and ceftriaxone-conjugated SNPs against ceftriaxone-resistant human pathogens, eg, *Bacillus cereus, Staphylococcus aureus, Klebsiella pneumoniae*, and *Pseudomonas aeruginosa*, the ceftriaxone-conjugated SNPs showed high inhibitory action than the unconjugated SNPs. However, many important approaches studied the antimicrobial effect of green synthesized SNPs using marine organisms, eg, Pugazhendhi et al[14] studied the effect of SNPs synthesized from the red algae *Gelidium amansii* against pathogenic Gram-positive bacteria: *S. aureus, Bacillus pumilus*, and Gram-negative bacteria: *Escherichia coli, P. aeruginosa, Vibrio parahaemolyticus, Aeromonas hydrophila*, which reduced the bacterial growth via exerting a bactericidal activity against the Gram-positive and Gram-negative bacterial pathogens. Also, Saravanan et al[15] reported the formation of SNPs using the fungus *Phenerochaete chrysosporium* that exhibited remarkable bactericidal activity against synthesized *P. aeruginosa, Klebsiella pneumonia, S. aureus,* and *Staphylococcus epidermidis* at a high dose.[16] Chitosan/cobalt-silica (Co-MCM) nanocomposites represent a new form of nanoparticles used for adsorption of various dyes like methyl orange, acridine orange, indigo carmine, and congo red and have high antibacterial potential against Gram-positive and Gram-negative bacteria as well as multi-drug resistant bacteria.[17–19] Also, Chitosan/CuO nanocomposite spheres have the ability to adsorb pollutants from water containing dyes and can inhibit the growth of *P. aeruginosa*.[20–22] Kavitha et al[23] synthesized cobaltosic oxide nanoparticles (Co3O4NPs) through a novel method and investigated its antibacterial activity along with the possible antibacterial activity against *E. coli*, where Co3O4NPs synthesized by one-step residue free in-situ thermal decomposition and Co3O4NPs were found to be highly efficient in killing *E. coli* via cell wall deterioration, which was evidenced by field emission scanning electron microscopy. The potent antibacterial activity of Co3O4NPs was found to be due to the electrostatic attraction between the bacterial cell and Co3O4NPs and further production of reactive oxygen species production by Co3O4NPs, which leads to intracellular oxidative stress and cell death.

In addition to the antimicrobial activity of nanoparticles, it is well known that nanoparticles opened a new field of nanomedicine in cancer therapy, where the structural and physical properties of SNPs give them a unique power for targeting and penetrating the abnormal cancer cell. As they can penetrate the abnormal cells causing DNA damage and determine defects in the genes.[24] SNPs can also aid in drug delivery, imaging of abnormal cells, and monitoring of therapeutic drugs against cancer.[24] The SNPs synthesized from the root extract of *Phoenix dactylifera* was found to control the growth of *Candida albicans* and *E. coli* on solid nutrient medium, and importantly SNPs were also found to decrease the cell viability of MCF-7 cell line and could act as a controller for human breast cancer.[25] All the previous studies showed that SNPs have multifunctioning properties and can be used as a therapeutic agent against cancer and infectious diseases.[25] Recently the green synthesis of SNPs using seaweeds gained high research attention and also gained a high concern in the biomedical applications. Ramkumar et al[26] used the extract of the seaweed *Enteromorpha compressa* to synthesize and stabilize the nanoparticles, and the synthesized SNPs showed efficient bactericidal activity against five human bacterial pathogens: *E. coli, K. pneumoniae, Pseudomonas sp., S. aureus*, and *Salmonella paratyphi* and fungal pathogens: *Aspergillus flavus, A. niger, A. ochraceus, A. terreus*, and *Fusarium moniliforme*. It also showed adequate cytotoxic activity against Ehrlich ascites carcinoma. It has been also reported that the SNPs synthesized using *Argyreia nervosa* leaves extract displayed strong antibacterial activity against food-borne bacteria, *E. coli*, and *S. aureus*, as well as antidiabetic and antioxidant potential.[27]

Concerning the antiviral activity of SNPs and their mechanism of action are not yet fully understood, very few studies have been found to investigate their activity against different viruses.[28,29] And although green synthesis of nanoparticles has attracted great attention in the last few decades, there is a lack of biological studies concerning the biological activity of the green synthesized SNPs from *L*ampranthus *coccineus* and *Ma*lephora *lutea*. Our approach is novel due to it aims to investigate and compare the possible antiviral activity of the aqueous and hexane extracts of *L. coccineus* and *M. lutea*, along with investigating the phytochemical composition of the crude methanolic extracts of the two plants through UPLC-MS metabolomic profiling, followed by molecular docking in order to explore the chemical compounds that might contribute to the antiviral potential.

Materials and methods

Plant material

The aerial parts of *L. coccineus* and *M. lutea* were collected in September 2016 from Engineer Ahmed Helal farm, Sheikh Zayed, Cairo, Egypt, and authenticated by senior botanist Mrs Therris Labib head specialist for plant identification at El-Orman botanical garden, Giza, Egypt. The two plants were washed with tap water at first, then surface washed with distilled water until no impurities remained. The clean aerial parts were shade dried for 20 days at room temperature to remove moisture. The dried aerial parts were pulverized in a clean electric blender to obtain a fine powder and stored in an airtight, amber glass bottle to avoid sunlight for further use.

Chemicals

All the reagents purchased were of analytical grade and used without any further purification. Silver nitrate ($AgNO_3$) was purchased from Sigma-Aldrich, Germany with ≥99.5%. Hexane, dimethylsulfoxide (DMSO), and anhydrous sodium sulfate were purchased from Al-Nasr Company for chemical industries for the preparation of hexane extracts, and distilled water was used for the preparation of aqueous extracts all over the experiments.

Synthesis of SNPs

Synthesis of SNPs using aqueous plant extract

SNPs were synthesized by macerating 10 g of the air-dried powder of *L. coccineus* and *M. lutea* aerial parts in 100 mL distilled water in a water bath at 60°C for 30 mins. Then, extract is filtered by Whatman no. 1 filter paper. For the biosynthesis of SNPs, the aqueous extract is added to 1 mM silver nitrate in the ratio 2:10 and kept in a water bath for 10 mins at 60°C.[30]

Synthesis of SNPs using hexane plant extract

The air-dried powder of *L. coccineus* and *M. lutea* aerial parts (100 g) was soaked in methanol and subsequently extracted with equal volumes of methanol (3×80 mL), the methanolic extract is filtered and evaporated on the rotary evaporator, Buchi, A.G., Switzerland. The dried methanol extracts of *L. coccineus* and *M. lutea* was then suspended in water and successively partitioned with equal volumes of *n*-hexane (3×50 mL). The hexane fraction was pooled and dried over anhydrous sodium sulfate, and the evaporated using rotary evaporator. SNPs were synthesized by adding 3 mL of 0.1% hexane fraction of *L. coccineus* and *M. lutea* in DMSO to 100 mL of 1 mM silver nitrate at room temperature.[31]

Metabolomic profiling of *L. coccineus* and *M. lutea* extracts

Metabolomic profiling was performed on methanolic extracts of *L. coccineus* and *M. lutea* according to Abdelmohsen et al[32–34] on an Acquity Ultra Performance Liquid Chromatography system coupled to a Synapt G2 HDMS quadrupole time-of-flight hybrid mass spectrometer (Waters, Milford, USA). Chromatographic separation was carried out on a BEH C18 column (2.1×100 mm, 1.7 µm particle size; Waters, Milford, USA) with a guard column (2.1×5 mm, 1.7 µm particle size) and a linear binary solvent gradient of 0–100% eluent B over 6 mins at a flow rate of 0.3 mL min^{-1}, using 0.1% formic acid in water (v/v) as solvent A and acetonitrile as solvent B. The injection volume was 2 µL and the column temperature was 40°C. To convert the raw data into separate positive and negative ionization files, MSConvert software was used. The files were then imported to the data mining software MZmine 2.10 for peak picking, deconvolution, deisotoping, alignment and formula prediction 11. The database used for the identification of compounds was the Dictionary of Natural Products 2015.

Antiviral activity

Antiviral activity was evaluated using MTT assay according to (Sethi, 2016; Andrighetti-Fröhner et al, 2003).[35,36]

VERO cells

VERO cells were purchased from Vacsera Research Foundation, Agouza, Giza, Egypt.

Determination of samples cytotoxicity on VERO cells

Different concentration from the tested samples were prepared, growth medium was decanted from 96-well microtiter plates after confluent sheet of VERO cell was formed, cell monolayer was washed twice with wash media, double-fold dilutions of tested sample was made in minimum essential media, 0.1 mL of each dilution was tested in different wells leaving three wells as control, receiving only maintenance medium, plate was incubated at 37°C and examined frequently for up to 2 days. Cells were checked for any physical signs of toxicity, eg, partial or complete loss of the monolayer, rounding, shrinkage, or cell granulation.

MTT solution was prepared as 5 mg/mL in PBS (BIO BASIC CANADA INC). 20 µL MTT solution was added to each well, then placed on a shaking table, 150 rpm for 5 mins, to thoroughly mix the MTT into the media. Incubated at (37° C, 5% CO2) for 1–5 hrs to allow the MTT to be metabolized, then dump off the media is done (dry plate on paper towels to remove residue if necessary). And formazan is re-suspended in 200 µL DMSO, placed on a shaking table, 150 rpm for 5 mins, to thoroughly mix the formazan into the solvent. The optical density is determined at 560 nm and the background is subtracted at 620 nm. Optical density should be directly correlated with cell quantity. The maximum non toxic concentration (MNTC) of each extract was determined and was used for further biological studies (Table S2 and Figure S2).[35,36]

MTT assay protocol

The antiviral activity was evaluated using MTT assay 10,000 cells plated in 200 µL media per well in a 96-well plate. Three wells are left empty for blank controls, incubated at (37°C, 5% CO_2) overnight to allow the cells to attach to the wells, then incubated equal volume (1:1 v/v) of nonlethal dilution of the tested sample and the virus suspension for 1 hr, 100 µL are added from viral/ sample suspension, placed on a shaking table at 150 rpm for 5 mins. The viral/sample suspension is incubated at (37ºC, 5% CO_2) for 1 day to allow the virus to take effect. 2 mL or more of MTT solution per 96-well plates at 5 mg/mL are made in PBS, the 20 µL MTT solution is added to each well, placed on a shaking table at 150 rpm for 5 mins, to thoroughly mix the MTT into the media. After that the plate is incubated at (37°C, 5% CO_2) for 1–5 hrs to allow the MTT to be metabolized, then the media is dumped off (dry plate on paper towels to remove residue if necessary). Formazan (MTT metabolic product) is re-suspended in 200 µL DMSO, placed on a shaking table, 150 rpm for 5 mins, to thoroughly mix the formazan into the solvent. The optical density is determined at 560 nm and the background is subtracted at 620 nm. Optical density should be directly correlated with cell quantity.[35,36]

Characterization of the synthesized SNPs by TEM

A drop of the SNPs solution was placed on a copper grid and coated with carbon support film. After drying, the shape and size of SNPs were analyzed using Transmission Electron Microscope (TEM) Jeol model JEM-1010, USA at The Regional Center for Mycology and Biotechnology, Al-Azhar University, Cairo, Egypt.

Characterization of the synthesized SNPs by UV-visible spectrometer and Fourier transform infrared spectroscopy (FTIR)

The formation of SNPs was monitored by measuring the UV–Vis spectrum of the reaction medium using a double beam V-630 spectrophotometer, Jasco, Japan, at the wavelength range from 200 to 600 nm at the Faculty of Pharmacy, Ain-Shams University, Cairo, Egypt.

FTIR-8400S, IR Prestige-21, IR Affinity-1, Shimadzu, Japan at Faculty of Pharmacy, Cairo University, Cairo, Egypt, was used for characterization of the functional group attached to the surface of SNPs.

Molecular docking

Three crystal structures were selected to study the antiviral activity of the compounds from the extract. The first crystal structure (PDB ID: 1KI2) is for the thymidine kinase of herpes simplex virus type I, which is a phosphotransferase enzyme involved in DNA synthesis and cell division. The active site in the 1KI2 crystal was defined according to the co-crystallized thymidine kinase inhibitor named Ganciclovir. The second crystal structure (PDB ID: 1QA7) is for 3C proteinase of hepatitis A virus with a co-crystallized inhibitor that was used to define the active site. The third crystal structure (PDB ID: 2ZU3) is for the 3c protease of coxsackievirus B4, which is essential for protein catabolism. The binding site for 2ZU3 was defined via a co-crystallized inhibitor, TG-0204998. Hence, three docking sites were used to study the binding patterns and affinities of the ligands. In all dockings, a grid box of dimensions 50 grid points and spacing 0.375 was centered on the given co-crystallized ligand. Four conformations were

generated for each ligand using OpenBabel, and docking was performed via Autodock4 implementing 100 steps of the genetic algorithm while keeping all the default settings provided by Autodock Tools. Visualization was done using the Discovery studio.

Results and discussion

Synthesis and characterization of SNPs

The aqueous and hexane extracts of *L. coccineus* and *M. lutea* were treated with 1 mM AgNO3 which resulted in changing the color of the aqueous and hexane extracts to reddish-brown which is the early sign for SNPs formation as shown in (Figure S1).

TEM characterization of the synthesized SNPs

The TEM analysis of SNPs of *L. coccineus* aqueous and hexane nano extracts showed spherical nanoparticles with mean size ranges between 10.12 and 27.89 nm, and for *M. lutea* the mean size ranges between 8.91 and 14.48 nm (Figure 1A–D).

UV-visible and FTIR characterization of the synthesized SNPs of *L. coccineus* and *M. lutea* aqueous and hexane extracts

The formation of SNPs was monitored by measuring the UV-Vis spectrum of the reaction medium in the wavelength range from 200 to 600 nm. SNPs were synthesized by

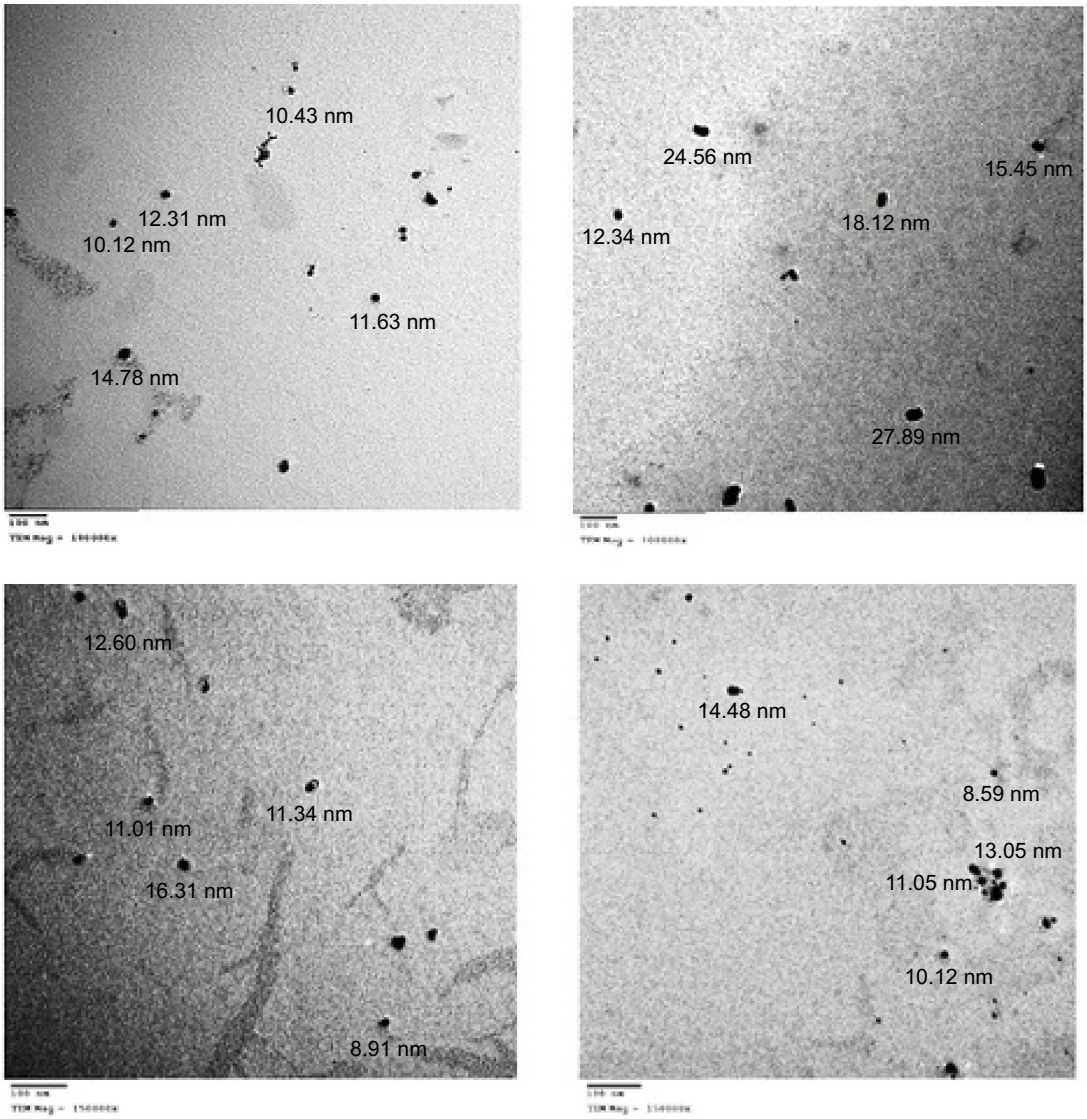

Figure 1 TEM photos for shape and size of produced SNPs of (**A**) aqueous extract of *Lampranthus coccineus*, (**B**) hexane extract of *Lampranthus coccineus*, (**C**) aqueous extract of *Malephora lutea*, (**D**) hexane extract of *Malephora lutea.*

Abbreviations: TEM, transmission electron microscope; SNPs, silver nanoparticles.

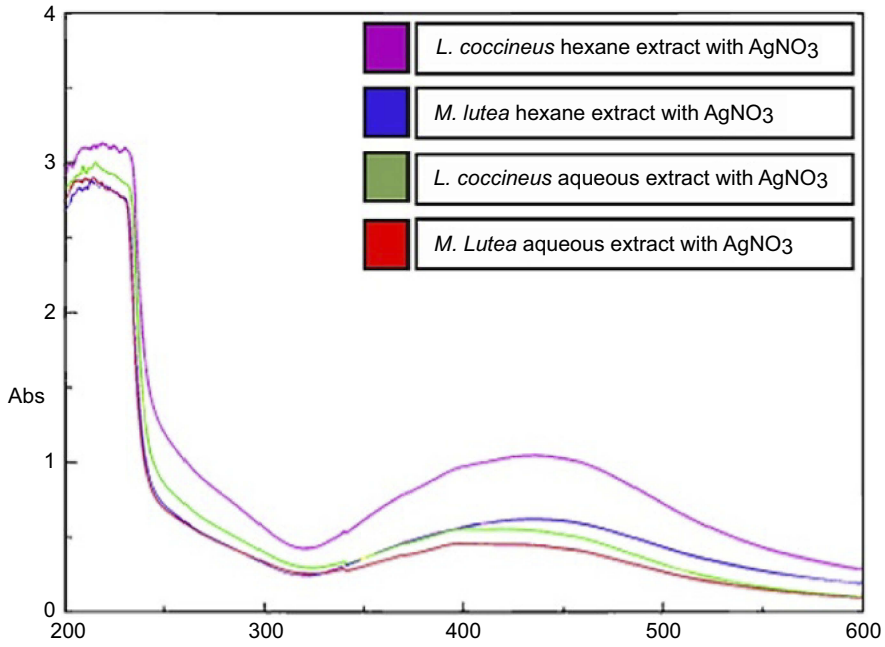

Figure 2 UV-Vis spectral analysis and color intensity of the biosynthesized SNPs of *Lampranthus coccineus* and *Malephora lutea* aqueous and hexane extract with $AgNO_3$.

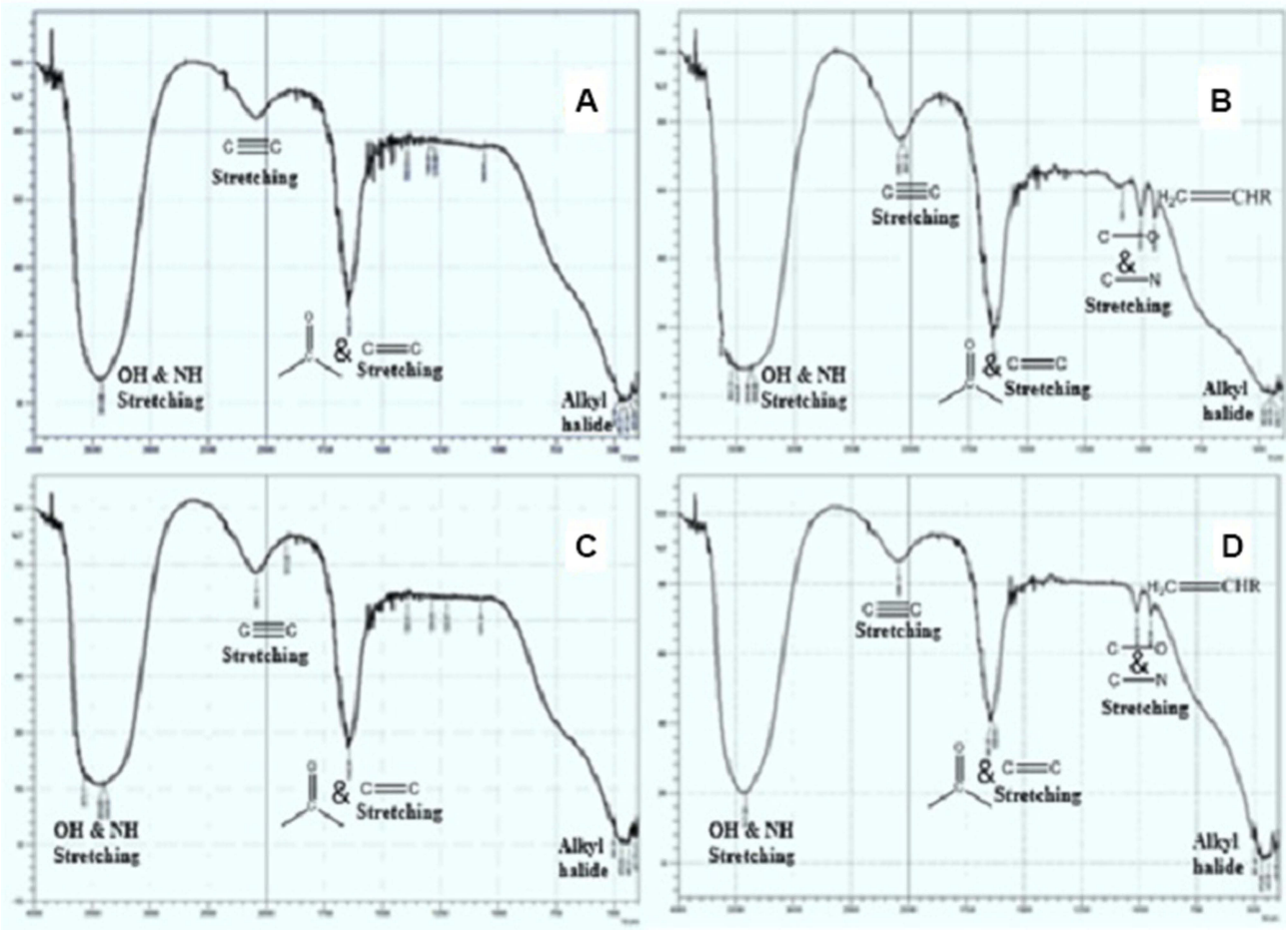

Figure 3 FTIR spectra after synthesis of nanoparticles of (**A**) *Lampranthus coccineus* aqueous extract, (**B**) *Lampranthus coccineus* hexane extract, (**C**) *Malephora lutea* aqueous extract, (**D**) *Malephora lutea* hexane extract.

adding 2 mL of the aqueous extracts of *L. coccineus* and *M. lutea* to 10 mL 1 mM of silver nitrate, and 0.3 mL of 0.1% hexane plant extract in DMSO to 10 mL of 1 mM silver, then the formed nanoparticles were analyzed by UV spectra. An absorbance band was observed at 417 nm, which are similar to those reported in the literature.[37] Mainly *L. coccineus* and *M. lutea* aqueous and hexane extracts showed absorbance peak at 417 nm, which confirms the formation of SNPs (Figure 2).

FTIR is used to characterize the functional groups attached to the surface of the nano metal particles, and it can identify the biomolecules responsible for capping and efficient stabilization of the metal nanoparticles.[38]

FTIR spectrum shows different major peak positions at 3,572.17, 3,421.72, 3,414, 3,390.86, 2,083.12, 1,913.39, 1,643.35, 1,635.64, 1,392.61, 1,284.59, 1,222.87, 1,246.02, 1,222.87, 1076.28, 505.35, 470.63, 450.06, 435.91 and 428.20 cm^{-1} (Figure 3A–D).

The peaks in the range of 3,200–3,500 cm^{-1} were assigned as –OH stretching in alcohols and phenolic compounds with strong hydrogen bonds and stretching of the N-H group also emerged in this range. The peak in the range 2,083.12 cm^{-1} is relevant to triple bond stretching. The FTIR peak in the range of 1,643.35 cm^{-1} indicates the C=O bond of the carbonyl group, C=C bond stretching and the stretching vibrations of amides also emerged in this range, while the peak in the range 1,392.61 cm^{-1} indicates the presence of a tertiary amide, C-N stretching and N-H bending. FTIR peaks appeared in the range 1,300–1,199.72 cm^{-1} is relevant to C-O stretching, 1,068.56–1,060.85 cm^{-1} demonstrates the presence of C-N aliphatic bond stretch, while the peaks in the range 505.35 cm^{-1} demonstrate bromo alkanes and the peaks in the range 482.20–428.20 cm^{-1} demonstrate alkyl halides bond stretch.[39]

The observed peaks are mainly attributed to alkaloids, terpenoids, flavonoids, glycosides, phenols, tannins, with functional groups such as ketone, aldehyde, hydroxyl group, and others. The presence of these groups increases the stability of the nanoparticles.[40]

These metabolites prevent clotting and pairing of the nanoparticles. The similarity between the spectra with some marginal shifts in peak position clearly indicates the presence of the residual plant extract in the sample as a capping agent to the

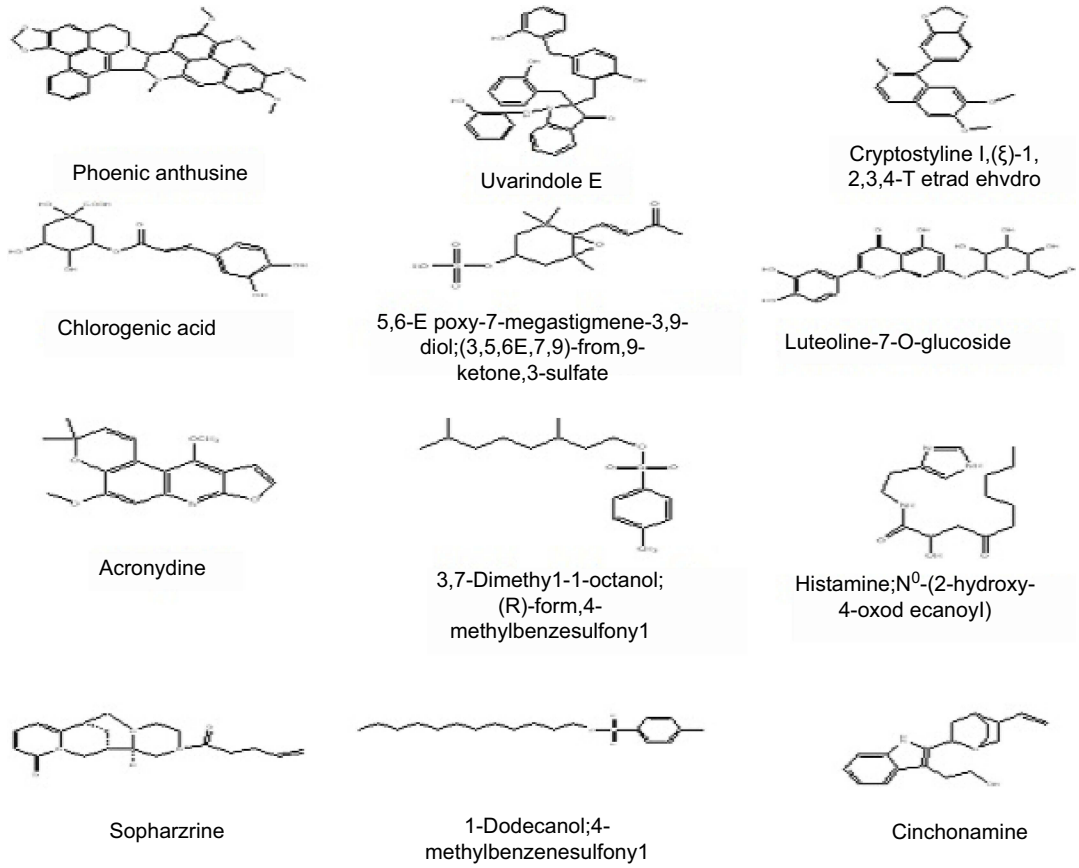

Figure 4 Compounds identified and dereplicated from the methanolic extract of *Lampranthus coccineus* and *Malephora lutea*.

Table 1 Cytotoxic effect of *Lampranthus coccineus* and *Malephora lutea* extracts on HAV-10, HSV-1, and CoxB4 virus

Tested extract	HAV-10 virus IC_{50} (µg/mL)	HSV-1 virus IC_{50} (µg/mL)	CoxB4 virus IC_{50} (µg/mL)
$AgNO_3$	NA	5.28	NA
Lampranthus coccineus aqueous nano extract	NA	520.6	NA
Lampranthus coccineus hexane nano extract	11.71	36.36	12.74
Malephora lutea hexane extract	NA	NA	46.44
Malephora lutea hexane nano extract	31.38	NA	29.04

Abbreviation: NA, no activity.

SNPs. Therefore, it may be inferred that these biomolecules are responsible for the capping and efficient stabilization of synthesized nanoparticles.

Metabolomic profiling of the crude methanolic extracts of *L. coccineus* and *M. lutea*

Dereplication of the secondary metabolites from the crude methanolic extract of *L. coccineus* and *M. lutea* resulted in the identification of different classes of compounds. The negative mode has the majority of the identified compounds and revealed the presence of various alkaloids, flavonoids, and phenolic compounds (Table S1 and Figure 4).

Antiviral activity

In order to ensure that the tested SNPs concentrations are not toxic, cytotoxicity of nanoparticles was assessed on VERO cell using MTT assay. The maximum non toxic concentration (MNTC) of $AgNO_3$ is 5.28 µg/mL, *L. coccineus* and *M. lutea* aqueous extracts 781.2 and 390.6 µg/mL, respectively, while the MNTC of the aqueous nano extracts of *L. coccineus* and *M. lutea* is 520.6 and 260.3 µg/mL. For the hexane extract of *L. coccineus* and *M. lutea*, the MNTC is 750 µg/mL, while for the nano hexane extracts it is 46.87 µg/mL for *L. coccineus* and *M. lutea.*

Using MTT antiviral assay protocol, the antiviral and cytotoxicity of the samples on HAV-10, HSV-1, and CoxB4 viruses were studied. The hexane nano extract of *L. coccineus* showed high antiviral activity against the HAV-10 virus with IC_{50} equal to 11.71 ng/mL, HSV-1 virus with IC_{50} equal to 36.36 µg/mL and CoxB4 virus with IC_{50} equal to 12.74 µg/mL. The aqueous nano extract of *L. coccineus* showed weak antiviral activity against HSV-1 with IC_{50} equal to 520.6 µg/mL and showed no antiviral activity against HAV-10, and CoxB4 viruses. The

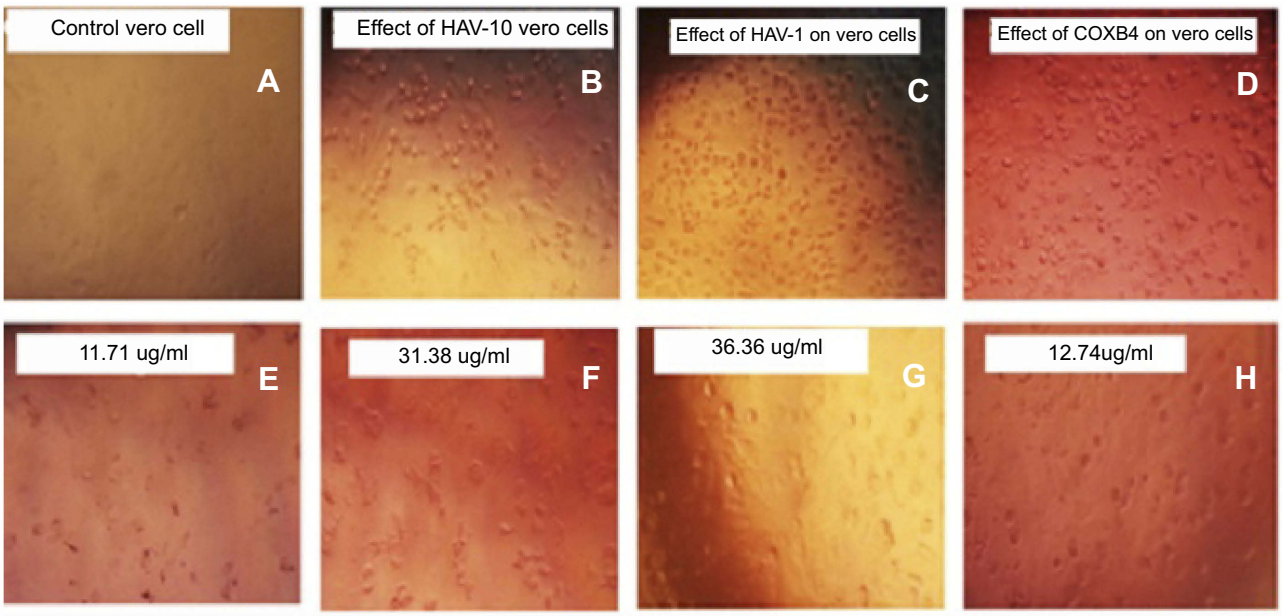

Figure 5 (**A**) Control Vero cell, (**B**) effect of HAV-10 virus on Vero cell, (**C**) effect of HSV-1 virus on Vero cell, (**D**) effect of COXB4 virus on Vero cell, (**E**) effect of *Lampranthus coccineus* hexane nano extract against HAV-10 virus (11.71 µg/mL), (**F**) effect of *Malephora lutea* hexane nano extract against HAV-10 virus (31.38 µg/mL), (**G**) effect of *Lampranthus coccineus* hexane nano extract against HSV-1 virus (36.36 µg/mL), (**H**) effect of *Lampranthus coccineus* hexane nano extract against COXB4 virus (12.74 µg/mL).

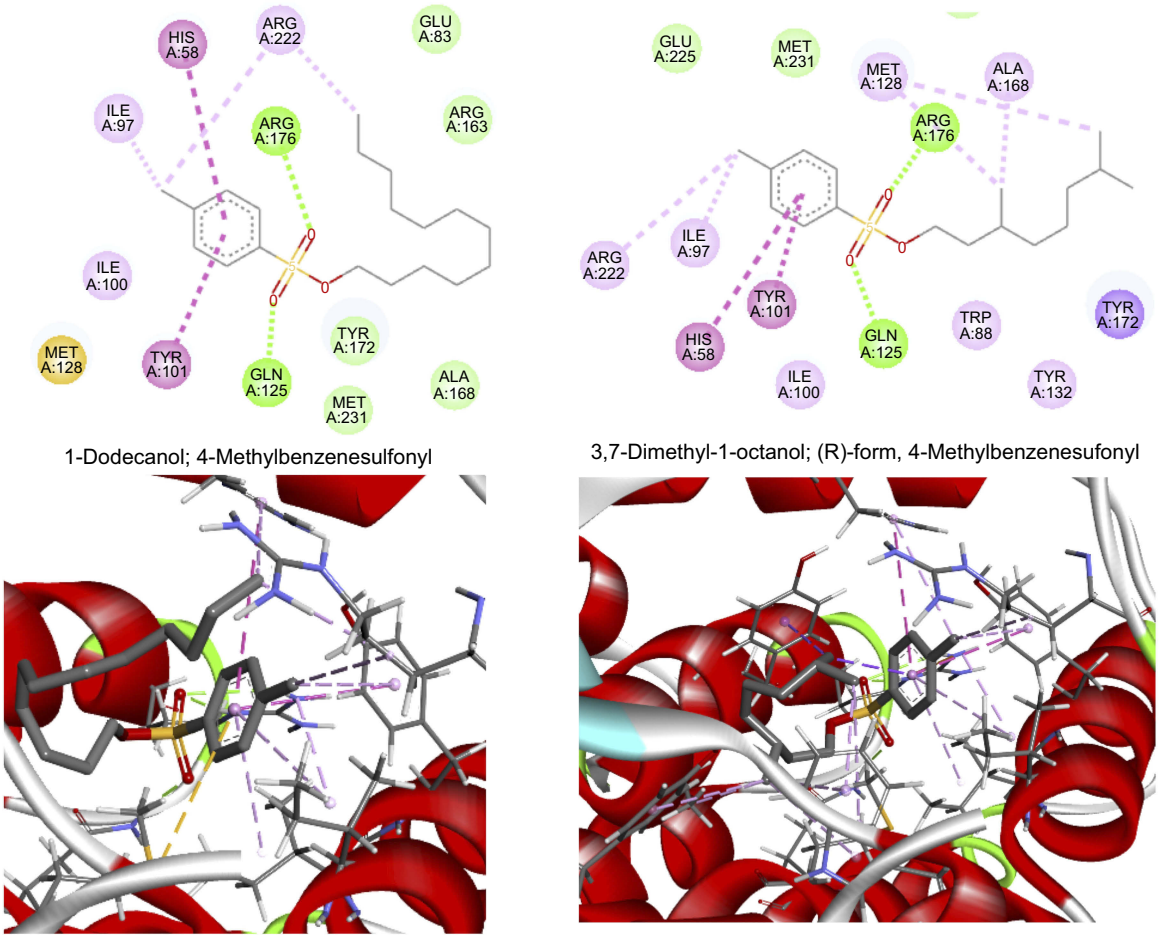

Figure 6 The interactions between two top-scoring ligands and the amino acids of the active site of the herpes simplex thymidine kinase (PDB ID: 1K12) depicted in 2D (top) and 3D (bottom). H-bonds, hydrophobic, and π-π stacking interactions are shown as green, light pink, and dark pink dotted lines, respectively.
Abbreviation: PDB, protein data bank.

hexane and aqueous extract of *L. coccineus* showed no antiviral activity against the three viruses. The hexane extract of *M. lutea* showed remarkable antiviral activity against the HAV-10 virus with IC50 equal to 31.38 µg/mL, the CoxB4 virus with IC_{50} equal to 29.04 µg/mL, and showed no antiviral activity against HSV-1 virus. The aqueous, aqueous nano, and hexane extracts of *M. lutea* showed no antiviral activity against HAV-10, HSV-1, and CoxB4 viruses. $AgNO_3$ also showed antiviral activity only against HSV-1 with IC_{50} equal to 5.13 µg/mL (Tables 1, S3, S4, S5 and Figures S3, 5A–H).

Molecular docking

Docking was performed in an attempt to rationalize the observed antiviral activity of the extract. The docking poses of all ligands in each protein were visually investigated against the co-crystallized ligands. Only the poses, which overlap with the co-crystallized ligands, were considered in the analysis. With herpes simplex thymidine kinase (PDB ID: 1KI2), the co-crystallized inhibitor (Ganciclovir) interactions include hydrogen bonds with Glu83, Gln125, Arg176, and Arg162. Other significant interactions included π-π stacking with Tyr172. With the two top ligands (Figure 6) similar interactions can be observed. These interactions include hydrogen bonds with Gln125 and Arg176 and π-π stacking with the neighboring Tyr101. The observed stacking, however, is of the T-shaped fashion in contrast to the parallel-spaced stacking observed with Ganciclovir (Table S6 and Figure 6).

The non-covalent interactions of the co-crystallized ligand of hepatitis A 3c proteinase (PDB ID: 1QA7) with the protein include van der Waals interactions in addition to hydrogen bond interactions with Val28, His145, and Cys172. Having lots of hydrophilic functional groups, the top two compounds in our docking study exhibit a myriad of hydrogen bonds with the protein, including those with His145, and Cys172. As illustrated in Figure 7, the compounds are predicted to have hydrogen bonds with Lys146, Lys 147, Gly170, Phe48, Lys50, Asn124, and Pro169. In addition, there is a predicted π-π stacking with Phe148 (Table S6 and Figure 7).

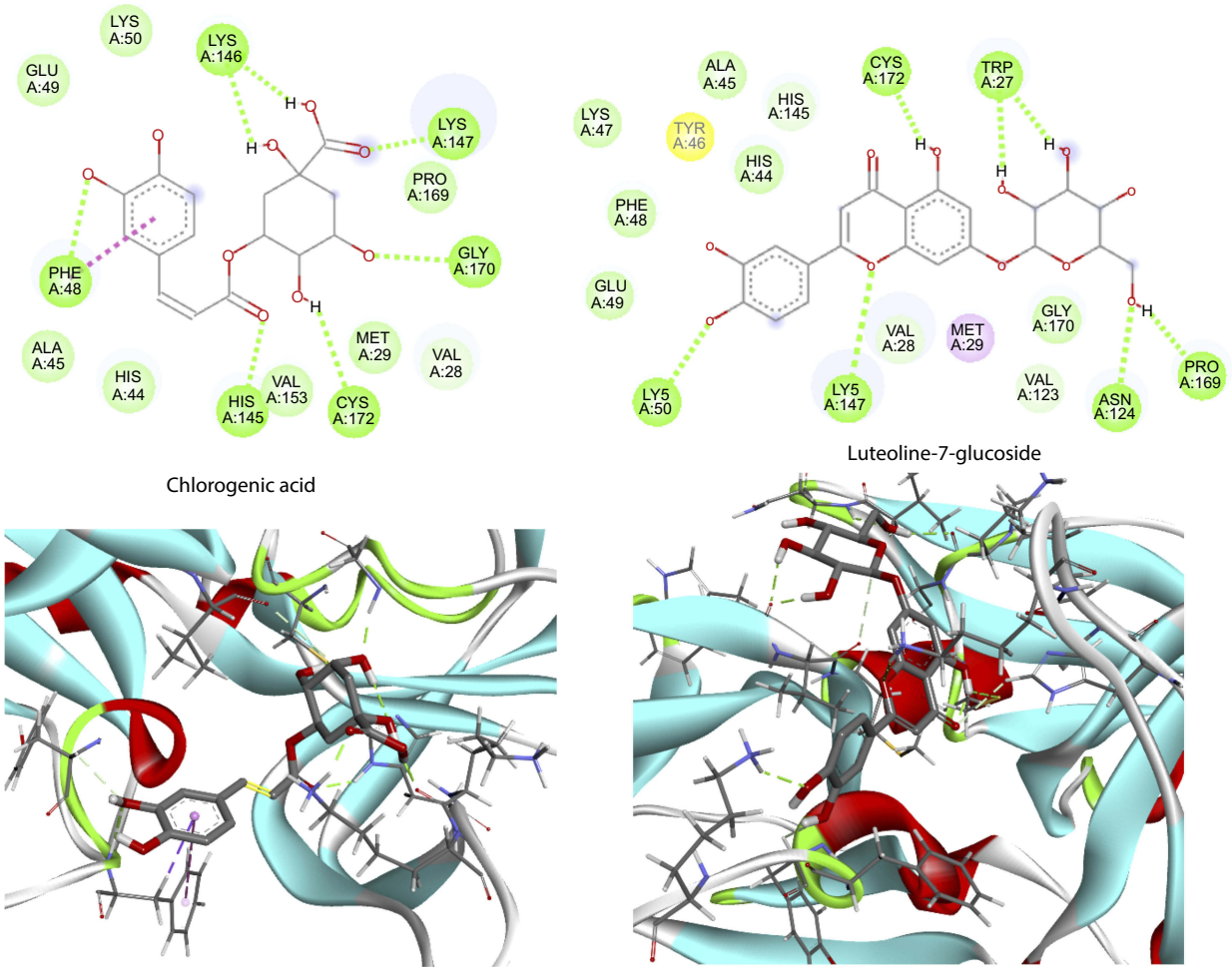

Figure 7 The interactions between two top-scoring ligands and the amino acids of the active site of hepatitis A 3c proteinase (PDB ID: 1QA7) depicted in 2D (top) and 3D (bottom). H-bonds are shown as green dotted lines.
Abbreviation: PDB, protein data bank.

The interactions of Coxsackievirus B4 3c protease (PDB ID: 2ZU3) with its co-crystallized inhibitor include hydrogen bonds with Thr142, Gly145, Arg143, His161, Gly164, and Thr142. As depicted in Figure 8, the top-scoring ligands exhibit a very similar network of hydrogen bonds with the neighboring amino acids (Table S6 and Figure 8).

The docking study predicts patterns of interactions between the compounds of *L. coccineus* and *M. lutea* with several viral proteins. These patterns are equivalent to those exhibited by known co-crystallized inhibitors. Therefore, this in silico study serves to provide an explanation for the observed antiviral activity.

Discussion

The SNPs were synthesized using the aqueous and hexane extracts of *L. coccineus* and *M. lutea*. Initially, the formation of SNPs was confirmed by observing the color change of the reaction mixture. The appearance of a reddish-brown color after 24 hrs of incubation at room temperature suggested the formation of SNPs.[41]

Similar findings were made by Jaidev and Narasimha.[42] SNPs are reddish-brown due to excitation of surface plasmon and its vibrations.[43] The reduction of silver ions in the silver nitrate solution upon addition of the aqueous and hexane extracts of *L. coccineus* and *M. lutea* manifests in the color change and leads to the formation of SNPs. The exact mechanism responsible for the synthesis of SNPs is yet to be known in detail, however, there is a hypothesis which supposes that the presence of secondary metabolites in plants makes a redox reaction and can be exploited for the biosynthesis of nanoparticles. These metabolites are responsible for the formation and stabilization of the biosynthesized nanoparticles.[44] The reduction of Ag+ ions was observed in the UV-visible spectrum. The size and shape of the SNPs can

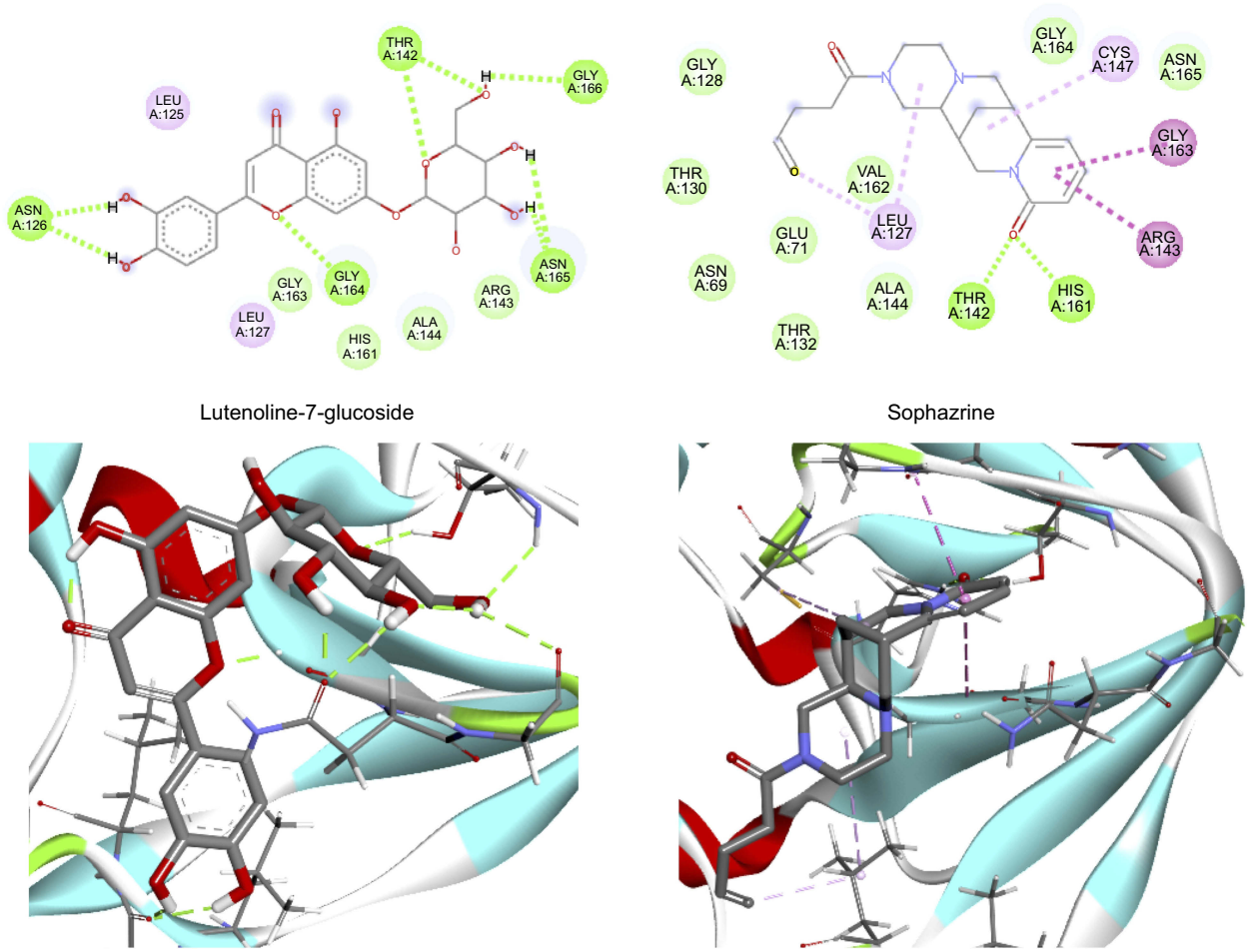

Figure 8 The interactions between two top-scoring ligands and the amino acids of the active site of Coxsackievirus B4 3c protease (PDB ID: 2ZU3) depicted in 2D (top) and 3D (bottom). H-bonds, hydrophobic, and δ^+-π stacking interactions are shown as green, light pink, and dark pink lines, respectively.
Abbreviation: PDB, protein data bank.

reflect the absorbance peak. The size of the nanoparticles has a linear correlation with the peak intensity. The results obtained from the present study confirm the formation of spherical nanoparticles with a mean size range between 10.12 and 27.89 nm estimated using TEM. FTIR results showed that the active constituents present in the plant extracts that are known to interact with Ag+ via functional groups and mediate the reduction to nanoparticles Ag^o.[38]

Medicinal plants contain a variety of natural compounds, which have strong antiviral activity. Green synthesized SNPs can further improve the therapeutic applicability of plants and can be a source of new antiviral agents.[45] These SNPs are safe and have multivalent functions, which make it less likely to encounter resistant viruses.[46]

The present study reports the green synthesis of SNPs using *L. coccineus* and *M. lutea* aqueous and hexane extracts and their application in inhibition of HAV-10, HSV-1, and CoxB4 infection. According to the results obtained, the biosynthesized SNPs of *L. coccineus* hexane extract enhanced the antiviral activity against the three tested viruses, while *M. lutea* hexane nano extract exhibited antiviral activity against only two viruses HAV-10 and CoxB4. SNPs showed significant inhibition of viral infection when incubated with viruses before the infection. Although the antiviral mechanism of action of green synthesized SNPs has not been determined, the antiviral activity of SNPs against several types of viruses is most probably due to binding of SNPs to viral envelope glycoproteins, thereby preventing the viral penetration into the host cell.[46,47] SNPs also may get access to the viral cell and exert their antiviral activity through interaction with viral genome (RNA or DNA) or via inhibiting the pathways that are essential for viral replication and it has been reported also that SNPs exhibit antiviral activity against numerous viruses, such as herpes simplex virus,[48] hepatitis B,[47] and H1N1 influenza. The performed docking study predicts patterns of

interactions between the compounds of *L. coccineus* and *M. lutea* with herpes simplex thymidine kinase, hepatitis A 3c proteinase, and Coxsackievirus B4 3c protease, which was similar to those of the co-crystal inhibitors and this can provide a supposed explanation for the antiviral activity of the aqueous and nano extracts of *L. coccineus* and *M. lutea*. The high efficacy of green synthesized nanoparticles gives new hope for finding new antiviral therapeutics against mutant and highly resistant viruses, and the mechanism of action should be further investigated to develop more efficient antiviral therapeutics.

Conclusion

From the present survey, it was observed that the green synthesized SNPs were capable of controlling the HAV-10 virus, HSV-1 virus, and CoxB4 virus infectivity. The nano hexane extract of *L. coccineus* is highly reactive as an antiviral agent against the three tested viruses HAV-10 virus, HSV-1 virus, and CoxB4 virus, while *M. lutea* hexane nano extract exhibited antiviral activity against only two viruses HAV-10 and CoxB4. These results highlight that SNPs could be used to inhibit and protect from viral infectivity, but further studies are required to determine the toxicity and the safety of the use of SNPs without creating any risk to human.

Acknowledgments

The authors are gratefully acknowledged to senior botanist Mrs Therris Labib head specialist for plant identification at El-Orman botanical garden, Giza, Egypt for authentication of the plant species under study.

Disclosure

The authors report no conflicts of interest in this work.

References

1. Singh T, Shukla S, Kumar P, Wahla V, Bajpai V, Rather I. Application of nanotechnology in food science: perception and overview. *Front Microbiol*. 2017;8:1–7. doi:10.3389/fmicb.2017.00001
2. Khan I, Saeed K, Khan I. Nanoparticles: properties, applications, and toxicities. *Arabian J Chem*. 2017;1:1–24.
3. Haider A, Kang IK. Preparation of silver nanoparticles and their industrial and biomedical applications: a comprehensive review. *Adv Mater Sci Eng*. 2015;1–16. doi:10.1155/2015/165257
4. Tran QH, Nguyen VQ, Le AT. Silver nanoparticles: synthesis, properties, toxicology, applications, and perspectives. *Adv Nat Sci*. 2013;4:1–20.
5. Shameli K, Ahmad MB, Zamanian A, et al. Green biosynthesis of silver nanoparticles using *Curcuma longa* tuber powder. *Int J Nanomedicine*. 2012;7:5603–5610. doi:10.2147/IJN.S30631
6. Jyoti K, Baunthiyal M, Singh A. Characterization of silver nanoparticles synthesized using *Urtica dioica* Linn. leaves and their synergistic effects with antibiotics. *J Radiat Res Appl Sci*. 2016;9(3):217–227. doi:10.1016/j.jrras.2015.10.002
7. Abou El-Nour KM, Eftaiha A, Al-Warthan A, Ammar RA. Synthesis and applications of silver nanoparticles. *Arab J Chem*. 2010;3:135–140. doi:10.1016/j.arabjc.2010.04.008
8. Lara HH, Garza-Trevino EN, Ixtepan-Turrent L, Singh DK. Silver nanoparticles are broad-spectrum bactericidal and viricidal compounds. *J Nanobiotechnol*. 2011;9:30. doi:10.1186/1477-3155-9-30
9. Marambio-Jones C, Hoek EV. A review of the antibacterial effects of silver nanomaterials and potential implications for human health and the environment. *J Nanopart Res*. 2010;12:1531–1551. doi:10.1007/s11051-010-9900-y
10. Lara H, Ayala-Núñez N, Ixtepan Turrent L, Rodrĺguez Padilla C. Bactericidal effect of silver nanoparticles against multidrug-resistant bacteria. *World J Microbiol Biotechnol*. 2010;26:615–621. doi:10.1007/s11274-010-0385-8
11. Gajbhiye M, Kesharwani J, Ingle A, Gade A, Rai M. Fungus-mediated synthesis of silver nanoparticles and their activity against pathogenic fungi in combination with fluconazole. *Nanomedicine*. 2009;5:382–386. doi:10.1016/j.nano.2009.06.005
12. Jogee PS, Ingle AB, Gupta IR, Bonde SR, Rai MK. Detection and management of mycotoxigenic fungi in nuts and dry fruits. *Acta Hortic*. 2012;963:69. doi:10.17660/ActaHortic.2012.963.10
13. Shanmuganathan R, Muthukumar H, Pugazhendhi A, et al. An enhancement of antimicrobial efficacy of biogenic and ceftriaxone-conjugated silver nanoparticles: green approach. *Environ Sci Pollut Res*. 2018;25:10362–10370. doi:10.1007/s11356-017-9367-9
14. Pugazhendhi A, Prabakar D, Jacob J, Karuppusamy I, Saratale R. Synthesis and characterization of silver nanoparticles using *Gelidium amansii* and its antimicrobial property against various pathogenic bacteria. *Microb Pathog*. 2017;114:41–45. doi:10.1016/j.micpath.2017.11.013
15. Saravanan M, Arokiyaraj S, Lakshmi T, Pugazhendhi A. Synthesis of silver nanoparticles from *Phenerochaete chrysosporium* (MTCC787) and their antibacterial activity against human pathogenic bacteria. *Microb Pathog*. 2018;117:68–72. doi:10.1016/j.micpath.2018.02.008
16. Jacob J, John M, Jacob A, et al. Bactericidal coating of paper towels via sustainable biosynthesis of silver nanoparticles using *Ocimum sanctum* leaf extract. *Mater Res Express*. 2019;4(4):1–27.
17. Khan S, Khan S, Kamal T, Yasir M, Asiri A. Antibacterial nanocomposites based on chitosan/Co-MCM as a selective and efficient adsorbent for organic dyes. *Int J Biol Macromol*. 2016;91:744–751. doi:10.1016/j.ijbiomac.2016.06.018
18. Kamal T, Islam M, Khan S, Asiri A. Adsorption and photo-degradation assisted dye removal and bactericidal performance of ZnO/chitosan coating layer. *Int J Biol Macromol*. 2015;584–590. doi:10.1016/j.ijbiomac.2015.08.060
19. Kamal T, Anwar Y, Khan S, Chani M, Asiri A. Dye adsorption and bactericidal properties of TiO2/Chitosan coating layer. *Carbohydr Polym*. 2016;148:153–160. doi:10.1016/j.carbpol.2016.04.042
20. Khan S, Ali F, Kamal T, Anwar Y, Asiri A, Seo J. CuO embedded chitosan spheres as an antibacterial adsorbent for dyes. *Int J Biol Macromol*. 2016;88:113–119. doi:10.1016/j.ijbiomac.2016.03.026
21. Ali F, Khan S, Kamal T, Anwar Y, Alamry K, Asiri A. Bactericidal and catalytic performance of green nanocomposite based on chitosan/carbon black fiber supported monometallic and bimetallic nanoparticles. *Chemosphere*. 2017;188:588–598. doi:10.1016/j.chemosphere.2017.08.118
22. Ahmed M, Kamal T, Khan S, et al. Assessment of anti-bacterial Ni-Al/chitosan composite spheres for adsorption assisted photo-degradation of organic pollutants. *Curr Nanosci*. 2016;12(5):1–25.
23. Kavitha T, Haider S, Kamal T, Ul-Islam M. Thermal decomposition of the metal complex precursor as a route to the synthesis of Co_3O_4 nanoparticles: antibacterial activity and mechanism. *J Alloys Compd*. 2017;704:296–302. doi:10.1016/j.jallcom.2017.01.306
24. Pugazhendhi A, Edison T, Karuppusamy I, Kathirvel B. Inorganic nanoparticles: a potential cancer therapy for human welfare. *Int J Pharm*. 2018;539(1–2):104–111. doi:10.1016/j.ijpharm.2018.01.034

25. Oves M, Aslam M, Rauf M, et al. Antimicrobial and anticancer activities of silver nanoparticles synthesized from the root hair extract of *Phoenix dactylifera*. *Mater Sci Eng*. 2018;89:429–443. doi:10.1016/j.msec.2018.03.035
26. Ramkumar V, Pugazhendhi A, Gopalakrishnan K, et al. Biofabrication and characterization of silver nanoparticles using the aqueous extract of seaweed *Enteromorpha compressa* and its biomedical properties. *Biotechnol Rep*. 2017;14:1–7. doi:10.1016/j.btre.2017.02.001
27. Saratale G, Saratale R, Benelli G, et al. Anti-diabetic potential of silver nanoparticles synthesized with *Argyreia nervosa* leaf extract high synergistic antibacterial activity with standard antibiotics against foodborne bacteria. *J Clust Sci*. 2017;28:1709–1727. doi:10.1007/s10876-017-1179-z
28. Galdiero S, Falanga A, Vitiello M, Cantisani M, Marra V, Galdiero M. Silver nanoparticles as potential antiviral agents. *Molecules*. 2011;16:8894–8918. doi:10.3390/molecules16108894
29. Huy T, Thanha N, Thuya N, Chunga P, Hungb P, Lec A, Hanha N. Cytotoxicity and antiviral activity of electrochemical – synthesized silver nanoparticles against poliovirus. *Journal of Virological Methods*. 2017; 241: 52–57.
30. Dondaa R, Kudlea K, Alwalaa J, Miryalaa A, Sreedharb B, Rudraa P. Synthesis of silver nanoparticles using extracts of *Securinega leucopyrus* and evaluation of its antibacterial activity. *Int J Curr Sci*. 2013;7:1–8. ISSN 2250–1770.
31. Rajesh S, Patric Raja D, Rathi JM, Sahayaraj K. Biosynthesis of silver nanoparticles using *Ulva fasciata* (Delile) ethyl acetate extract and its activity against *Xanthomonas campestris* pv. malvacearum, Bionanoparticle for phytopathogen management. *JBiopest*. 2012.5: 119–128.
32. Abdelmohsen U, Cheng C, Viegelmann C, et al. Dereplication strategies for targeted isolation of new antitrypanosomal actinosporins A and B from a marine sponge-associated-*actinokineospora* sp. EG49. *Mar Drugs*. 2014;12:1220–1244. doi:10.3390/md12031220
33. Abdelhafez O, Fawzy M, Fahim J, et al. Hepatoprotective potential of *Malvaviscus arboreus* against carbon tetrachloride-induced liver injury in rats. *PLoS One*. 2018;13(8):1–18. doi:10.1371/journal.pone.0202362
34. Raheem D, Tawfike A, Abdelmohsen U, Edrada-Ebel R, Fitzsimmons-Thoss V. Application of metabolomics and molecular networking in investigating the chemical profile and antitrypanosomal activity of British bluebells (*Hyacinthoides non-scripta)*. *Sci Rep*. 2019;9:1–13. doi:10.1038/s41598-018-37186-2
35. Sethi P. Activity of *turbinaria ornata* (Turner) J. Agade against Blue Tongue Virus (Btv). *IOSR J Pharm*. 2016;6(7):93–95. Version. 3. doi:10.9790/3013-067039395
36. Andrighetti-Fröhner R, Antonio V, Creczynski-Pasa B, Barardi M, Simões O. Cytotoxicity and potential antiviral evaluation of violacein produced by *Chromobacterium violaceum*. *Mem Inst Oswaldo Cruz, Rio De Janeiro*. 2003;98(6):843–848. doi:10.1590/S0074-02762003000600023
37. Jose A, Abirami T, Kavitha V, Sellakilli R, Karthikeyan J. Green synthesis of silver nanoparticles using *Asystasia gangetica* leaf extract and its antibacterial activity against gram-positive and gram-negative bacteria. *J Pharmacogn Phytochem*. 2018;7(1):2453–2457.
38. Thomas B, Prasad A, Vithiya S. Evaluation of the antioxidant, antibacterial and photocatalytic effect of silver nanoparticles from methanolic extract of *Coleus vettiveroids*-an endemic species. *J Nanostruct*. 2018;8(2):179–190.
39. Kumar R, Ghoshal G, Jain A, Goyal M. Rapid green synthesis of silver nanoparticles (AgNPs) using (*Prunus persica*) Plants extract: exploring its antimicrobial and catalytic activities. *J Nanomed Nanotechnol*. 2017;8(4):1–8.
40. Erjaee H, Rajaian H, Nazifi S. Synthesis and characterization of novel silver nanoparticles using *Chamaemelum* nobile extract for antibacterial application. *Adv Nat Sci*. 2017;8:1–9.
41. Avilala J, Golla N. Antibacterial and antiviral properties of silver nanoparticles synthesized by marine actinomycetes. *Int J Pharm Sci Res*. 2019;10(3):1223–1228.
42. Jaidev R, Narasimha G. Fungal mediated biosynthesis of silver nanoparticles characterization and antimicrobial activity. *Colloids Surf B*. 2010;81:430–433. doi:10.1016/j.colsurfb.2010.07.033
43. Shankar S, Rai A, Ahmad A, Sastry M. Rapid synthesis of silver nanoparticles by using onion (*Allium cepa*) extract and their antibacterial activity. *Digest J Nanomater Biostruct*. 2004;5:427–432.
44. Gandhiraj V, Kumar. K, Madhusudhanan J, Sandhya J. Antitumor activity of biosynthesized silver nanoparticles from leaves of *Momordica charantia* against MCF-7 cell line. *Int J ChemTech Res*. 2015;8(7):351–362.
45. Galdiero S, Falanga A, Cantisani M, Ingle A, Galdiero M, Rai M. Silver nanoparticles as novel antibacterial and antiviral agents. *Front Nanomedical Re*. 2014:3;565–594.
46. Fatima M, Zaidi N, Amraiz D, Afzal F. In vitro antiviral activity of *Cinnamomum cassia* and its nanoparticles against H7N3 influenza A virus. *J Microbiol Biotechnol*. 2016;26(1):151–159. doi:10.4014/jmb.1508.08024
47. Kwon J, Kim H, Yoon Y, et al. In vitro inhibitory activity of *Alpinia katsumadai* extracts against influenza virus infection and hemagglutination. *Virol.J*. 2010;7:307. doi:10.1186/1743-422X-7-307
48. Ko C, Wei L, Chiou F. The effect of medicinal plants used in Chinese folk medicine on RANTES secretion by virus-infected human epithelial cells. *J Ethnopharmacol*. 2006;107:205–210. doi:10.1016/j.jep.2006.03.004